Supporting Information

Van Der Meer et al. 10.1073/pnas.1315657111

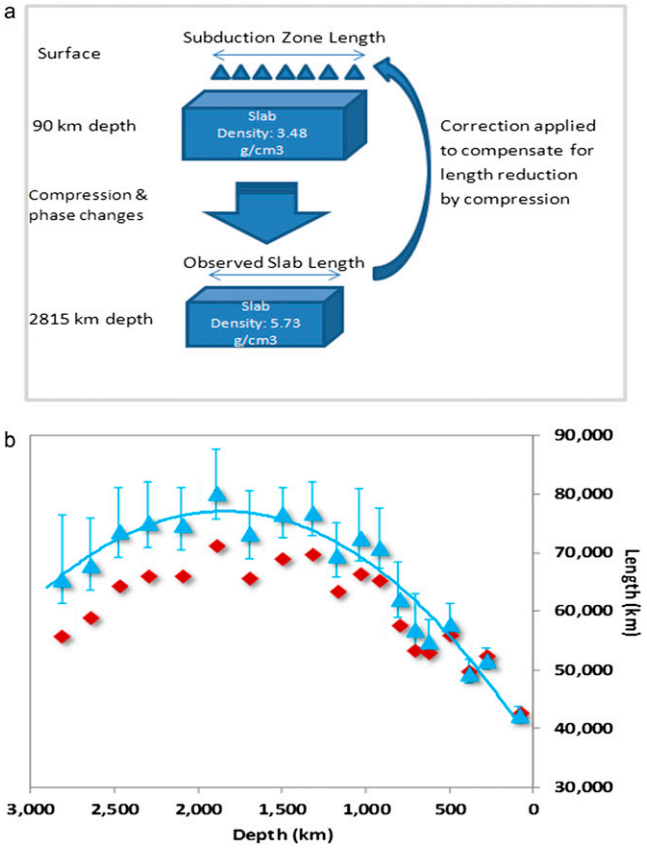

Fig. S1. Correction for volume reduction by self compression. (*A*) Schematic illustrating the correction from observed slab length to subduction-zone length by using the density model (1). (*B*) Graph illustrating the correction from slab (red diamonds) to subduction-zone length (blue triangles).

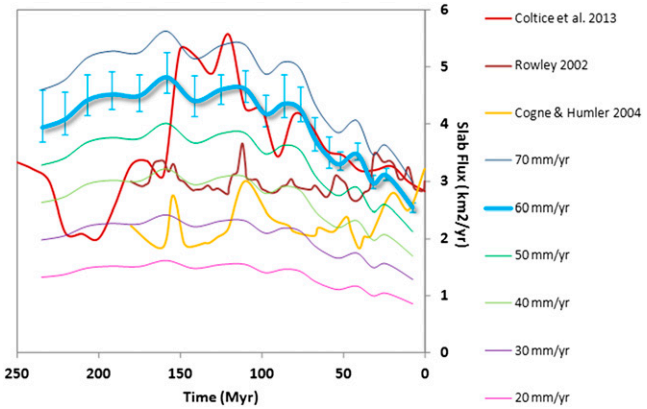

Fig. S2. Slab flux through time. Production rates by midoceanic ridges; ref. 2, red; ref. 3, brown; and ref. 4, yellow. Other lines represent the slab flux derived from our subduction length multiplied with various convergence velocities. Bold light-blue line is our best-fit estimate for slab flux including error bars, based on a convergence velocity of 6 cm/y.

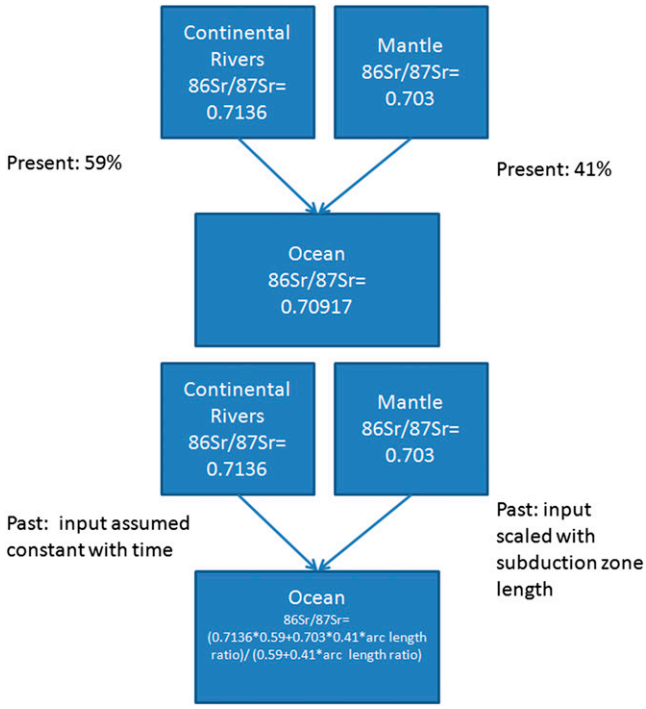

Fig. S3. Radiogenic strontium mixing model. Adapted from ref. 11. Paleooceanic $^{86}Sr/^{87}Sr$ ratios are calculated by scaling the mantle component with our derived subduction-zone length.

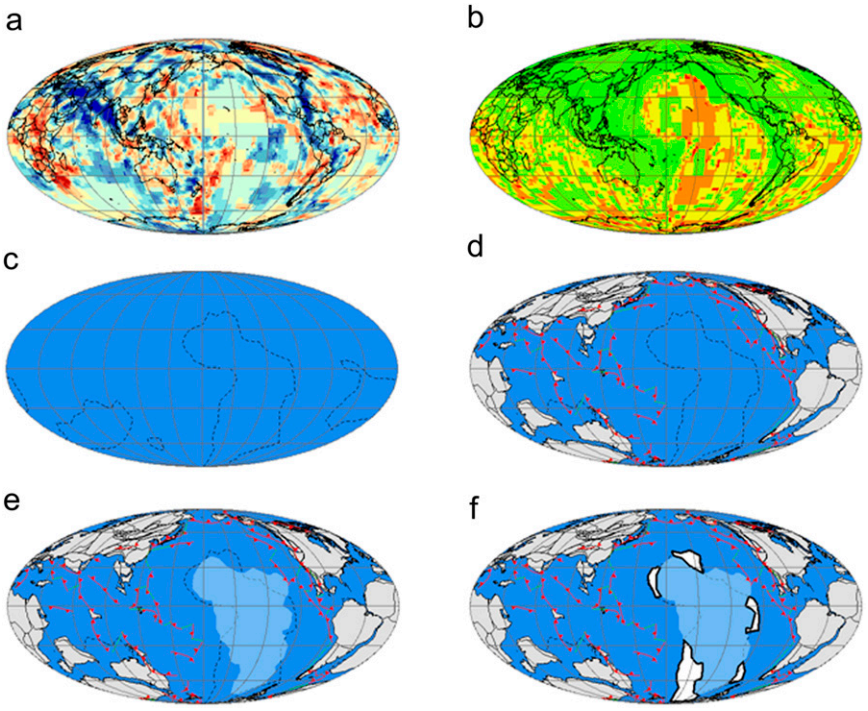

Fig. S4. Derivation of subduction-zone length error bounds. Example of (*A*) slice from tomographic model (5) at 1,500 km depth, and (*B*) hit count map (5) at 1,500 km depth. Red <100 ray paths/cell; orange (100–500 ray paths/cell); light green (1,000–5,000 ray paths/cell); dark green (5,000+ ray paths/cell); (*C*) dashed areas; poorly imaged zones (6, 7). (*D*) Plate tectonic reconstruction (6, 8, 9) of 120 Ma, subduction zone interpretations (6, 7) (red), poorly imaged zone (dashed). (*E*) Same as *C*, but with Pacific plates (light blue) with <10 My age uncertainty (10). (*F*) Remaining areas where slabs are possible, but not imaged (white).

1. Kennett BLN, Engdahl ER, Buland R (1995) Constraints on seismic velocities in the Earth from traveltimes. *Geophys J Int* 122(1):108–124.
2. Coltice N, Seton M, Rolf T, Müller RD, Tackley PJ (2013) Convergence of tectonic reconstructions and mantle convection models for significant fluctuations in seafloor spreading. *Earth Planet Sci Lett* 383:92–100.
3. Rowley DB (2002) Rate of plate creation and destruction: 180 Ma to present. *Geol Soc Am Bull* 114(8):927–933.
4. Cogné J-P, Humler E (2004) Temporal variation of oceanic spreading and crustal production rates during the last 180 My. *Earth Planet Sci Lett* 227(3-4):427–439.
5. Amaru ML (2007) Global travel time tomography with 3-D reference models. PhD dissertation (University of Utrecht, Utrecht, Netherlands).
6. van der Meer DG, Spakman W, van Hinsbergen DJJ, Amaru ML, Torsvik TH (2010) Towards absolute plate motions constrained by lower-mantle slab remnants. *Nat Geosci* 3:36–40.
7. van der Meer DG, Torsvik TH, Spakman W, van Hinsbergen DJJ, Amaru ML (2012) Intra-Panthalassa Ocean subduction zones revealed by fossil arcs and mantle structure. *Nat Geosci* 5:215–219.
8. Torsvik TH, Müller RD, Van der Voo R, Steinberger B, Gaina C (2008) Global plate motion frames: Toward a unified model. *Rev Geophys* 46(3):1–44.
9. Steinberger B, Torsvik TH (2008) Absolute plate motions and true polar wander in the absence of hotspot tracks. *Nature* 452(7187):620–623.
10. Müller RD, Sdrolias M, Gaina C, Steinberger B, Heine C (2008) Long-term sea-level fluctuations driven by ocean basin dynamics. *Science* 319(5868):1357–1362.
11. Allegre CJ, et al. (2010) The fundamental role of island arc weathering in the oceanic Sr isotope budget. *Earth Planet Sci Lett* 292(1):51–56.

Table S1. Slab data table

		Slab depth				Slab midpoint		
		Base		Top				
Abbreviation	Slab name	Min	Max	Min	Max	Depth	Lon	Lat
Aeg	Aegean Tethys	2,100	1,900	0	0	1,000	26.0	42.0
Ag	Algeria	2,300	2,100	1,500	1,325	1,806	7.0	24.0
Al	Aleutian	810	710	0	0	380	−165.0	57.0
At	Atlantis	2,900	2,815	2,650	2,480	2,711	−39.0	22.0
Ba	Balkan	2,900	2,815	2,650	2,480	2,711	17.0	47.0
Bf	Beaufort	2,815	2,650	2,300	2,100	2,466	−128.0	72.0
Ca	Caribbean	810	710	0	0	380	−63.0	13.0
CC	Central China	2,900	2,815	1,500	1,325	2,135	88.0	45.0
Ch	Chukchi	1,900	1,700	1,175	1,040	1,454	170.0	77.0
EC	East China	2,900	2,815	1,700	1,500	2,229	128.0	43.0
Eg	Egypt	2,300	2,100	920	810	1,533	31.0	32.0
Far	Farallon	2,650	2,480	920	710	1,690	−73.0	35.0
GI	Georgia Islands	2,900	2,815	1,500	1,325	2,135	−30.0	−56.0
Hi	Himalayas	1,175	1,040	500	440	789	78.0	26.0
Id	Idaho	2,480	2,300	810	710	1,575	−118.0	49.0
Kc	Kamchatka	1,040	920	0	0	490	155.0	55.0
Mc	Manchuria	1,040	920	0	0	490	135.0	46.0
Md	Maldives	2,100	1,900	560	500	1,265	79.0	14.0
Me	Mesopotamia	2,300	2,100	1,325	1,175	1,725	46.0	33.0
Mg	Mongolia	2,100	1,900	1,175	1,040	1,554	120.0	48.6
MO	Mongol-Okhotsk	2,900	2,815	1,900	1,700	2,329	76.0	67.0
NP	North Pacific	1,500	1,325	850	760	1,109	−143.0	56.0
Ro	Rockall	2,900	2,815	2,650	2,480	2,711	−13.0	57.0
Sa	Sakhalin	1,175	1,040	710	625	888	135.0	55.4
So	Socorro	2,300	2,100	810	710	1,480	−108.0	17.0
TA	Trans Americas	2,900	2,815	2,480	2,300	2,624	−67.0	2.0
Ve	Venezuela	1,500	1,325	810	710	1,086	−67.0	2.0
Wc	Wichita	2,815	2,650	2,100	1,900	2,366	−98.0	37.0
Te1	Telkhinia1	2,480	2,300	2,100	1,900	2,195	178.0	14.0
Te2	Telkhinia2	2,300	2,100	1,700	1,500	1,900	179.0	5.0
Te3	Telkhinia3	1,700	1,500	1,500	1,175	1,469	−177.0	−2.0
Te4	Telkhinia4	2,900	2,815	2,300	2,100	2,529	164.0	34.0

Table S2. Subduction-zone length data

Depth (km)	Age (My)	Lateral slab length (km)	Tomographic spatial error (km)	Slab count	Shrinkage factor	SBZ length	SBZ length error (km)	Poor imaging zones error (km)	Combined error root sum of squares	SBZ length ratio average	SBZ length ratio minimum	SBZ length ratio maximum
90	8	42,672	200	23	0.99	42,426	1,349	0	1,349	1.000	0.968	1.032
285	24	52,465	200	28	0.99	51,686	1,474	1,410	2,040	1.218	1.184	1.266
385	32	49,770	200	33	0.99	49,478	1,615	1,787	2,409	1.166	1.128	1.223
500	42	55,992	200	33	1.03	57,925	1,681	3,007	3,445	1.365	1.326	1.447
628	52	53,119	200	31	1.03	54,936	1,629	3,423	3,791	1.295	1.256	1.384
710	59	53,469	400	26	1.07	57,021	3,076	5,182	6,026	1.344	1.272	1.486
810	68	57,784	400	27	1.08	62,160	3,162	5,654	6,478	1.465	1.391	1.618
920	77	65,464	400	35	1.09	71,032	3,631	5,548	6,631	1.674	1.589	1.831
1,040	87	66,544	400	39	1.09	72,641	3,856	7,609	8,530	1.712	1.621	1.913
1,175	98	63,464	400	34	1.10	69,644	3,620	4,425	5,717	1.642	1.556	1.776
1,325	110	69,785	400	40	1.10	77,013	3,948	3,500	5,276	1.815	1.722	1.940
1,500	125	69,095	400	42	1.11	76,736	4,071	1,895	4,491	1.809	1.713	1.915
1,700	142	65,688	400	47	1.12	73,459	4,337	5,842	7,276	1.731	1.629	1.903
1,900	158	71,381	400	49	1.13	80,352	4,457	5,903	7,397	1.894	1.789	2.068
2,100	175	66,158	400	47	1.13	74,941	4,393	4,516	6,300	1.766	1.663	1.915
2,300	192	66,119	400	46	1.14	75,345	4,372	5,244	6,827	1.776	1.673	1.937
2,480	207	64,357	400	48	1.15	73,714	4,489	5,986	7,482	1.737	1.632	1.914
2,650	221	59,097	400	43	1.15	68,004	4,269	6,843	8,065	1.603	1.502	1.793
2,815	235	55,934	400	39	1.17	65,659	4,147	10,235	11,043	1.548	1.450	1.808

SBZ, subduction-zone length.